

# Unified Treatment of Fluorescence and Raman Scattering Processes near Metal Surfaces

Hongxing Xu, Xue-Hua Wang, Martin P. Persson, and H. Q. Xu

*Division of Solid State Physics, Lund University, Box 118, S-221 00 Lund, Sweden*

Mikael Käll

*Department of Applied Physics, Chalmers University of Technology, S-412 96 Göteborg, Sweden*

Peter Johansson\*

*Department of Natural Sciences, University of Örebro, S-701 82 Örebro, Sweden*

(Received 5 March 2004; published 6 December 2004)

We present a general model study of surface-enhanced resonant Raman scattering and fluorescence focusing on the interplay between electromagnetic effects and the molecular dynamics. Our model molecule is placed close to two Ag nanoparticles and has two electronic levels. A Franck-Condon mechanism provides electron-vibration coupling. Using realistic parameter values for the molecule we find that an electromagnetic enhancement by 10 orders of magnitude can yield Raman cross sections  $\sigma_R$  of the order  $10^{-14}$  cm<sup>2</sup>. We also discuss the dependence of  $\sigma_R$  on incident laser intensity.

DOI: 10.1103/PhysRevLett.93.243002

PACS numbers: 33.20.Fb, 33.50.-j, 42.50.-p

Discovered nearly three decades ago, surface-enhanced Raman scattering (SERS) has developed into an extremely sensitive spectroscopic technique with, in some cases, single-molecule sensitivity [1–4]. It is well known that SERS, as well as a range of related surface-enhanced optical processes, mainly results from electromagnetic (EM) effects [5,6]. Although the Raman scattering cross section  $\sigma_R$  for a molecule in free space is very small (of the order of  $10^{-30}$  cm<sup>2</sup> for nonresonant,  $10^{-24}$  cm<sup>2</sup> for resonant scattering), the same molecule placed between two metal particles may well have an effective  $\sigma_R$  that is 10–12 orders of magnitude larger. The reason is that EM fields are strongly modified near and, in particular, between, metallic particles, so the local excitation field induced by an incident wave is much stronger there (by a factor that we denote  $M$ ) than in free space. Likewise, by virtue of electromagnetic reciprocity, the amplitude of the radiation sent out from a source near the particles is equally enhanced compared with a source in free space. Consequently, quantities such as the absorption cross section for a molecule increase by a factor  $|M|^2$ , whereas Raman scattering, which involves both an absorption and an emission event, increases by a factor  $|M|^4$ .

A large number of theory papers on surface-enhancement phenomena have focused on the electromagnetic aspects, but only a few have considered the molecular dynamics in more detail; see, for example, Ref. [7]. In this work we present a general model that treats the electromagnetic and molecular aspects on an equal footing. It includes photon-molecule coupling, coupling between electronic and vibrational degrees of freedom on the molecule, and radiative and nonradiative damping mechanisms [8], and is analyzed by means of a density-matrix calculation. The model lets us study not only how the molecule-metal-particle geometry affects

the EM enhancement and molecule damping rates, but also how these parameters in turn influence the spectrum of light emitted by the molecule. In particular, the model allows us to simultaneously quantify both scattering processes (Raman and Rayleigh) and fluorescence near metal surfaces, a field that has attracted a growing interest in recent years [9,10]. By applying the model to the case of a highly fluorescent molecule situated between silver nanoparticles, we obtain an effective Raman cross section of the same order of magnitude as in recent single-molecule SERS data [1,4]. In addition, we study the effects of a strong incident field, which drives the molecule out of thermal equilibrium, and predict that it is possible to observe effects such as anti-Stokes Raman scattering even at low temperatures.

Figure 1 schematically shows the main ingredients of the model. A molecule is placed on the symmetry axis between two spherical, metallic (Ag) nanoparticles. This

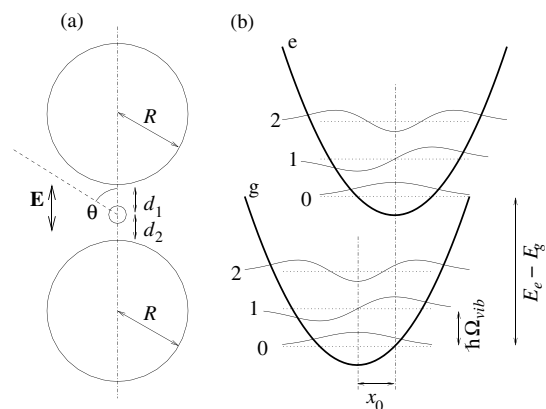


FIG. 1. Schematic illustration of (a) the model geometry, and (b) the oscillator potential governing the vibrational motion of the molecule in the electronic ground and excited states.

system is illuminated from the side ( $\theta = 90^\circ$ ) by a laser with light polarized along the symmetry axis. The scattered and fluorescent light is collected by a detector also placed on the side of the nanoparticle system.

We treat the molecule as an electronic two-level system with an excitation energy  $E_e - E_g = \hbar\Omega_{ge}$ . The model also includes one symmetric molecular vibration mode with frequency  $\Omega_{\text{vib}}$  and reduced mass  $\mu$ . The electronic and vibrational degrees of freedom are coupled by a Franck-Condon mechanism. As shown in Fig. 1 the equilibrium position of the vibrational coordinate is displaced a distance  $x_0$  upon electronic excitation. The dimensionless parameter  $\alpha = x_0/\sqrt{2\hbar/(\mu\Omega_{\text{vib}})}$  characterizes the strength of the electron-vibration coupling which ultimately makes Raman processes possible.

The spectrum (differential cross section per unit photon energy  $\hbar\omega$  and solid angle  $\Omega$ ) of the light sent out by the molecule in the direction of  $\theta = 90^\circ$  as a result of both scattering and fluorescence processes can be calculated from [11]

$$\frac{d^2\sigma}{d\Omega d(\hbar\omega)} = \frac{\omega^4 |M(\omega)|^2}{I_{\text{in}} 8\pi^3 c^3 \epsilon_0 \hbar} \text{Re} \int_0^\infty dt e^{i\omega t} \langle p^{(-)}(0) p^{(+)}(t) \rangle. \quad (1)$$

Here  $I_{\text{in}}$  is the incident laser intensity and  $M(\omega)$  is the EM enhancement factor. The normal-ordered correlation function  $\langle p^{(-)}(0) p^{(+)}(t) \rangle$  of the molecule dipole moment  $p$  can be evaluated by means of the quantum regression theorem [11] once we know the molecule's time-averaged density matrix and its equation of motion. In this way light emitted both as a result of molecular transitions (fluorescence) and as a result of the molecule's oscillating dipole moment (scattering) is accounted for. We calculate the density matrix  $\rho$  describing the molecule dynamics keeping a finite number  $N_{\text{vib}}$  (usually four) of vibrational levels per electronic level. The equation of motion reads

$$id\rho/dt = (1/\hbar)[H_{\text{mol}} + H', \rho] + \mathcal{L}_{\text{tr}}\rho + \mathcal{L}_{\text{ph}}\rho, \quad (2)$$

where  $H'$  describes the molecule-laser interaction,  $\mathcal{L}_{\text{tr}}$  and  $\mathcal{L}_{\text{ph}}$  account for various damping processes which we specify below, and  $H_{\text{mol}}$  is the molecule Hamiltonian,

$$H_{\text{mol}} = \sum_{n=0}^{N_{\text{vib}}-1} \sum_{l=g,e} |l; n\rangle (E_l + n\hbar\Omega_{\text{vib}}) \langle l; n|. \quad (3)$$

The molecule-electric-field interaction is a central ingredient in the dynamics that we account for by a  $-e\vec{r} \cdot \vec{E}$  term in the Hamiltonian. The electric field  $\vec{E}$  has contributions both from the incident laser beam and the vacuum fluctuations. The laser field

$$\vec{E}_L = \hat{z}E_0 \cos\Omega_L t = \hat{z}E_0 [e^{i\Omega_L t} + e^{-i\Omega_L t}]/2 \quad (4)$$

yields a transition matrix element (in the rotating-wave approximation) between two molecule states in the electronic ground and excited states, respectively,

$$\langle e; m | H' | g; n \rangle = -M(\Omega_L) p_0 E_0 e^{-i\Omega_L t} f(n, m)/2. \quad (5)$$

Here  $\hbar\Omega_L$  is the photon energy and  $p_0 = e\ell_{\text{dip}}$  is the transition dipole moment between the electronic states.  $f(n, m)$  is a Franck-Condon factor, i.e., the overlap  $f(n, m) = \langle 0; n | x_0; m \rangle$  between state  $|n\rangle$  in the undisplaced oscillator potential and state  $|m\rangle$  in the displaced potential, which depends on the parameter  $\alpha = x_0/\sqrt{2\hbar/(\mu\Omega_{\text{vib}})}$  introduced above [12].

For a molecule in free space the interaction with the EM vacuum fluctuations yields a decay rate from state  $|e; m\rangle$  to  $|g; n\rangle$  due to spontaneous emission [13],

$$\Gamma_{gn,em} = \omega^3 |p_0|^2 |f(n, m)|^2 / (3\pi\hbar\epsilon_0 c^3). \quad (6)$$

Near the metallic particles the decay rate is modified,  $\Gamma_{gn,em} \rightarrow |M_d(\omega)|^2 \Gamma_{gn,em}$ , where  $\omega = \Omega_{ge} + (m-n)\Omega_{\text{vib}}$ .  $|M_d|^2 = P/P_{\text{free}}$  is the ratio of the power emitted by a dipole placed at the position of the molecule with and without the metal particles present. Usually  $|M_d|^2$  is of a similar order of magnitude as  $|M|^2$ , yet the two factors may differ substantially because  $|M_d|^2$  accounts for radiation in all directions as well as energy dissipation in the metal particles. We calculate  $M$  and  $M_d$  using extended Mie theory [14]. The optical properties of the particles are represented by a tabulated, local dielectric function [15]. For small ( $< 20\text{--}30 \text{ \AA}$ ) molecule-particle separations  $d$ , there are important corrections ( $\sim 1/d^4$ ) to the damping-rate enhancement  $|M_d|^2$  as a result of electron-hole pair creation in the particles. To capture this we calculate, in the nonretarded limit while applying a long-wavelength cutoff, the power  $P_{\text{eh}}$  dissipated by the dipole when placed between two flat Ag samples (at the same distances as the spheres) whose optical properties are described by a nonlocal dielectric function based on  $d$ -parameter theory [16], and add this to the output power  $P_{\text{Mie}}$  found in the Mie calculation, i.e.,  $|M_d|^2 = (P_{\text{Mie}} + P_{\text{eh}})/P_{\text{free}}$ .

Decay and dephasing rates enter the last two terms of Eq. (2). Standard quantum optics methods [11] yield

$$\mathcal{L}_{\text{tr}}\rho = -\sum_{kj} \frac{i\Gamma_{kj}}{2} [\sigma_{jk}\sigma_{kj}\rho + \rho\sigma_{jk}\sigma_{kj} - 2\sigma_{kj}\rho\sigma_{jk}] \quad (7)$$

in the low-temperature limit. ( $\sigma_{kj}$  denotes a matrix with the only nonzero element  $kj$  equal to 1.)  $\Gamma_{kj}$  is the total decay rate from state  $j$  to  $k$ . It includes the radiative and nonradiative processes discussed above as well as vibrational damping due to transitions with a phenomenological rate  $\gamma_{\text{vib}}$  to the nearest, lower level within the same electronic state. We also introduce a phenomenological dephasing rate  $\gamma_{\text{ph}}$  that enters the last term of Eq. (2),  $\mathcal{L}_{\text{ph}}\rho_{kj} = -i\gamma_{\text{ph}}\rho_{kj}$  provided the electron states of  $k$  and  $j$  differ. Let us stress that  $\gamma_{\text{ph}}$  is brought into the model in order to broaden the fluorescence resonances of the molecule. In reality an organic molecule has many vibration modes and, therefore, an almost continuous fluorescence

spectrum. Dephasing gives us a broadened fluorescence spectrum even though the model molecule has only one vibrational mode. It has limited impact on the resonant Raman scattering as long as  $\gamma_{\text{ph}}$  is smaller than, or comparable to, the laser detuning.

The inset of Fig. 2 shows the absorption cross section  $\sigma_A$  and Raman profile ( $\sigma_R$  as a function of *incident* photon energy) calculated using the Fermi golden rule for the model molecule in free space [13]. The experimental absorption cross section for a Rhodamine 6G (R6G) dye molecule is shown in the same diagram. We have set the parameter values cited in the caption to obtain a similar spectrum.  $\hbar\Omega_{ge}$  gives the overall peak position and  $\hbar\Omega_{\text{vib}}$  the vibrational quantum, and the value for  $\gamma_{\text{vib}}$  is reasonable for a molecule at a metal surface.  $\alpha$  has been chosen to reproduce the shoulder of the spectrum, and  $\gamma_{\text{ph}}$  and  $\ell_{\text{dip}}$  were set to reproduce the width and height of the R6G spectrum, respectively. The free-molecule Raman cross section is 7 to 8 orders of magnitude smaller than  $\sigma_A$ , and its maximum is blueshifted compared with the absorption spectrum due to quantum-mechanical interference between processes with different intermediate vibrational states for the molecule.

The main panel in Fig. 2 shows spectra calculated with the model molecule placed between two silver spheres with radius  $R = 400 \text{ \AA}$  and three different, symmetric (i.e.,  $d_1 = d_2$  in Fig. 1) molecule-particle separations. All three spectra have a broad fluorescence peak around  $\hbar\Omega_{ge} = 2.3 \text{ eV}$ , which shifts to a slightly lower energy for  $d = 5 \text{ \AA}$  since the maximum of  $M$  is redshifted as the EM coupling between the Ag particles increases. In ad-

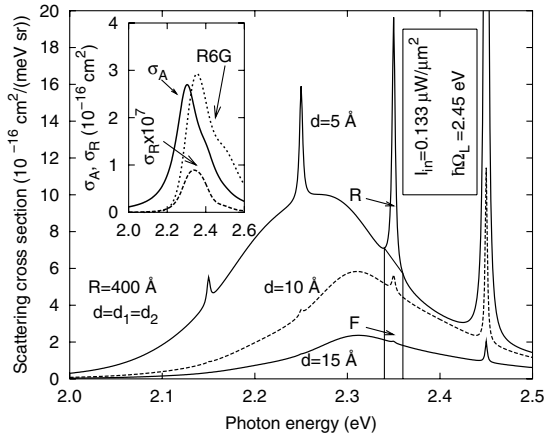


FIG. 2. Combined Raman and fluorescence spectra for a model molecule, with parameter values  $\hbar\Omega_{ge} = 2.3 \text{ eV}$ ,  $\hbar\Omega_{\text{vib}} = 0.1 \text{ eV}$ ,  $\gamma_{\text{ph}} = 10^{14} \text{ s}^{-1}$ ,  $\gamma_{\text{vib}} = 2 \times 10^{12} \text{ s}^{-1}$ ,  $\alpha = 0.5$ , and  $\ell_{\text{dip}} = 1 \text{ \AA}$ , placed between two Ag particles with  $R = 400 \text{ \AA}$  for three different molecule-particle separations, and  $\hbar\Omega_L = 2.45 \text{ eV}$ . Inset: the absorption and Stokes Raman scattering cross sections  $\sigma_A$  and  $\sigma_R$  as a function of the *incident* laser photon energy for the model molecule in *free space*. The experimental  $\sigma_A$  for an R6G molecule is shown as a comparison.

dition a number of sharp peaks emerge, due to either Rayleigh scattering off the molecule (at  $2.45 \text{ eV}$ ) or Raman scattering (redshifted by multiples of  $\hbar\Omega_{\text{vib}} = 0.1 \text{ eV}$  from  $2.45 \text{ eV}$ ).  $\sigma_R$  varies rapidly when the geometry is changed; for  $d = 5 \text{ \AA}$  the Raman peaks are comparable in height to the fluorescence background, whereas for  $d = 15 \text{ \AA}$  the Raman peak is barely discernible; cf. Ref. [17].

The EM enhancement  $|M|$  grows with decreasing  $d$  yielding a rapid growth of the Raman signal which involves both an absorption and an emission event and thus scales as  $\sim |M|^4$ . Fluorescence also involves both photon absorption and emission, but the cross section in this case scales only as  $\sim |M|^4/|M_d|^2$ . The fluorescence intensity is proportional to the EM enhancement in emission,  $|M|^2$ , multiplied by the probability of finding the molecule in the excited state. This probability is relatively insensitive to the enhancement because it is set by the ratio ( $\sim |M/M_d|^2$ ) between the laser excitation rate and the deexcitation rate due to spontaneous emission.

Figure 3 shows the dependence of the Raman ( $\sigma_R$ ), fluorescence ( $\sigma_F$ ), and total ( $\sigma_T$ ) cross sections on the distance  $d$ , exhibiting the same general tendencies as discussed above.  $\sigma_F$  has been calculated from the area marked F in Fig. 2. For the Raman scattering we have plotted two curves: one is obtained from the area marked R in Fig. 2, but this calculation works only for relatively small  $d$ , so we also estimate  $\sigma_R$  by multiplying the free-molecule Raman cross section by the enhancement factor  $|M(\Omega_L)|^2|M(\Omega_L - \Omega_{\text{vib}})|^2$ . The estimate agrees well with the “peaks” result for  $d \approx 15\text{--}25 \text{ \AA}$  and, of course, gives the true result for larger  $d$ . For small  $d$  the two results differ, and here the peaks result is the true one; it includes

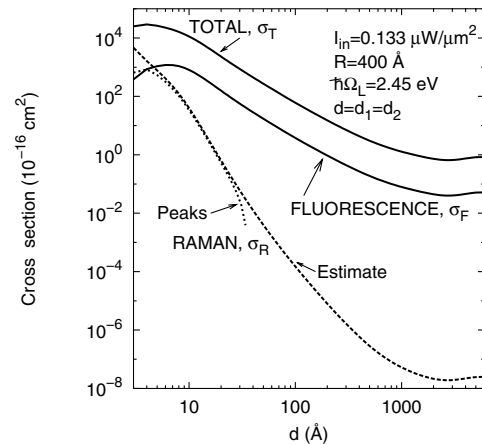


FIG. 3. Calculated cross sections as a function of molecule-metal-particle distance. The Raman (peaks) and fluorescence results have been extracted from the areas marked R and F, respectively, in Fig. 2 multiplied by the angular average  $8\pi/3$ . The “estimate” curve gives the free-molecule Raman cross section multiplied by the relevant enhancement factor  $|M(\Omega_L)|^2|M(\Omega_L - \Omega_{\text{vib}})|^2$ . The “total” curve is the total cross section integrated over the energy range  $1.5\text{--}2.8 \text{ eV}$ .

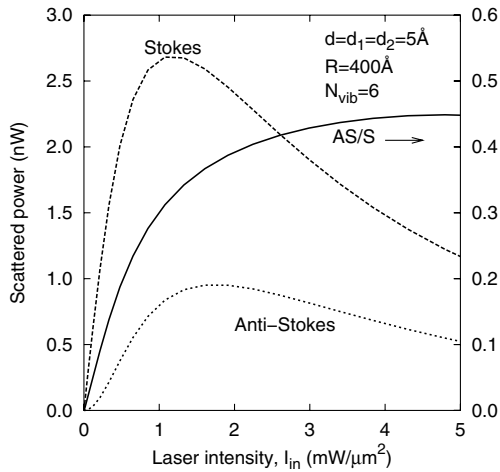


FIG. 4. Stokes and anti-Stokes Raman scattering power (for low temperature) as well as their ratio as a function of  $I_{in}$  calculated with the parameter values given in Fig. 2.

effects on the Raman scattering of the strong energy dissipation that are not included in the estimate.

At large  $d$  the cross sections approach those of a free molecule. The influence of the particles causes a weak interference phenomenon; there is a minimum in  $\sigma_R$  and  $\sigma_F$  at  $d \approx 3000 \text{ \AA}$ . For smaller  $d$ , both  $\sigma_R$  and  $\sigma_F$  increase as a result of EM enhancement. Over a range of distances the enhancement factors roughly scale as  $1/d$  meaning that  $\sigma_F \sim 1/d^2$  and  $\sigma_R \sim 1/d^4$ . At  $d \lesssim 30 \text{ \AA}$ , more complicated behavior sets in. Resonant enhancement with resonance frequencies that shift with changing geometry occurs, and damping effects become important. These first affect  $\sigma_F$  which in spite of an increasing enhancement  $M$  levels off around  $d = 10 \text{ \AA}$  and eventually decreases, because the molecule is usually deexcited through a nonradiative process. For the smallest distances  $\sigma_R$  becomes larger than  $\sigma_F$ , but it eventually decreases due to the strong dissipation which damps also the coherent oscillations of the molecular dipole moment.

In Fig. 4 we show results for the power of both Stokes and anti-Stokes Raman scattering as a function of incident laser intensity  $I_{in}$ . For low intensity, the Stokes power is linear in  $I_{in}$  (constant  $\sigma_R$ ) while the anti-Stokes power grows quadratically with  $I_{in}$ . The anti-Stokes signal occurs because in an intense laser field the molecule can be found in an excited vibrational level of the electronic ground state once the rate of electronic excitation and deexcitation becomes comparable to the vibrational damping rate  $\gamma_{vib}$ . The probability for the molecule being vibrationally excited is roughly  $C|M(\Omega_L)|^2\sigma_A\phi_{ph}/\gamma_{vib}$ , ( $C \lesssim 1$  is a numerical factor), and this ratio is  $\approx 0.6C$  with  $|M(\Omega_L)|^2 \approx 1.4 \times 10^5$  and  $I_{in} = 0.5 \text{ mW}/\mu\text{m}^2$  corresponding to a photon flux  $\phi_{ph} = 10^{23} \text{ photons}/(\text{cm}^2 \text{ s})$ . Note that in this model the excited vibrational state is pumped mainly by repeated

absorption and deexcitation rather than by Raman scattering [18,19]. For higher intensities both the Stokes and anti-Stokes signals saturate and eventually decrease. The molecule is driven so hard that its polarizability becomes time dependent. This happens when the effective Rabi frequency  $\Omega_R = M(\Omega_L)p_0E_0/\hbar$  becomes comparable to other relevant frequency scales, in our case the dephasing rate  $\gamma_{ph}$ . For the parameter values used here  $\Omega_R \approx 4 \times 10^{13} \text{ s}^{-1}$  at  $I_{in} = 0.5 \text{ mW}/\mu\text{m}^2$ .

In summary, we have presented a model calculation that treats surface-enhanced Raman scattering and fluorescence on an equal footing. We found that, with realistic parameter values, a resonant Raman cross section of  $\sim 10^{-14} \text{ cm}^2$  can be reached with an EM enhancement by 10 orders of magnitude. We also found that for an incident laser intensity of  $\sim 1 \text{ mW}/\mu\text{m}^2$  it is possible to get a considerable anti-Stokes Raman signal.

We acknowledge support from the Swedish Research Council and the Swedish Foundation for Strategic Research, and we thank Lars Samuelson for useful discussions.

\*Corresponding author.

- [1] S. Nie and S. R. Emory, *Science* **275**, 1102 (1997).
- [2] K. Kneipp *et al.*, *Phys. Rev. Lett.* **78**, 1667 (1997).
- [3] H. X. Xu, E. J. Bjerneld, M. Käll, and L. Börjesson, *Phys. Rev. Lett.* **83**, 4357 (1999).
- [4] A. M. Michaels, M. Nirmal, and L. E. Brus, *J. Am. Chem. Soc.* **121**, 9932 (1999).
- [5] M. Moskovits, *Rev. Mod. Phys.* **57**, 783 (1985); A. Otto, in *Light Scattering in Solids IV*, edited by M. Cardona and G. Guntherodt (Springer-Verlag, Berlin, 1984), p. 289.
- [6] J. I. Gersten and A. Nitzan, *Surf. Sci.* **158**, 165 (1985).
- [7] B. Pettinger, *J. Chem. Phys.* **85**, 7442 (1986).
- [8] Charge transfer processes between the metal particles and the molecule, which may also play a role in SERS, are beyond the scope of this model.
- [9] W. L. Barnes, *J. Mod. Opt.* **45**, 661 (1998).
- [10] J. R. Lakowicz, *Anal. Biochem.* **298**, 1 (2001).
- [11] M. O. Scully and M. Suhail Zubairy, *Quantum Optics* (Cambridge University Press, Cambridge, 1997).
- [12] The simplest Franck-Condon factors are given by  $f(0, 0) = e^{-\alpha^2/2}$ ,  $f(1, 1) = e^{-\alpha^2/2}(1 - \alpha^2)$ , and  $f(1, 0) = -f(0, 1) = \alpha e^{-\alpha^2/2}$ . For small  $\alpha$ ,  $\sigma_R \sim \alpha^2$ .
- [13] J. J. Sakurai, *Advanced Quantum Mechanics* (Addison-Wesley, Reading, MA, 1967).
- [14] H. X. Xu, J. Aizpurua, M. Käll, and P. Apell, *Phys. Rev. E* **62**, 4318 (2000).
- [15] E. D. Palik, *Handbook of Optical Constants of Solids* (Academic Press, New York, 1985).
- [16] A. Liebsch, *Phys. Rev. B* **36**, 7378 (1987).
- [17] K. Sokolov, G. Chumanov, and T. M. Cotton, *Anal. Chem.* **70**, 3898 (1998).
- [18] K. Kneipp *et al.*, *Phys. Rev. E* **57**, R6281 (1998).
- [19] T. L. Haslett, L. Tay, and M. Moskovits, *J. Chem. Phys.* **113**, 1641 (2000).